Modeling of Molecular Packing and Conformation in Oligofluorenes

Valentina Marcon,[†,‡] Nico van der Vegt,[†] Gerhard Wegner,[†] and Guido Raos*[,‡]

Max-Planck-Institut für Polymerforschung, Ackermannweg 10, D-55128 Mainz, Germany, and Dipartimento di Chimica, Materiali e Ingegneria Chimica "Giulio Natta", Politecnico di Milano, Via L. Mancinelli 7, I-20131 Milano, Italy

Received: November 25, 2005; In Final Form: January 30, 2006

We describe the application of molecular modeling to study problems related to the packing and conformation of oligofluorene molecules in the solid state. First of all, we describe an improved force field for oligofluorenes. The model is based on the MM3 force field for the intramolecular degrees of freedom, but it relies on ab initio calculations for the torsion potential between two monomers and the electrostatic interactions. We also report ab initio calculations of the interaction potentials between fluorene and fluorenone units. The force field has been tested on the crystal structures of a fluorene monomer, a dimer, and a pentamer containing a fluorenone at the center. It has then been employed to study conformational defects of the chains, both in vacuo and in the bulk. We find that certain modes of inversion from right-handed to left-handed helices are also possible within the constraining environment of the crystals. The effect of the presence of two different types of side chains has been also addressed. Finally, the possibility of having two fluorene units parallel and close to each other has been investigated as a model of a ground-state precursor of an excimer. Our simulations show that this configuration is sterically and energetically unfavorable so that formation of an excimer following optical excitation appears to be unlikely.

I. Introduction

Polyfluorenes form a class of conjugated polymers that have received much attention because of their promising performance in optical and electronic applications,[1−3] such as organic light-emitting diodes[4] and photovoltaic devices.[5] Excited polyfluorenes emit blue light with high quantum efficiency. Color tuning can be achieved by blending[6,7] or covalent linkage[8−10] of two components. Furthermore, because of their high-energy optical gap, they can serve as donors for electronic energy transfer to a lower energy acceptor.[2] It has been shown that film morphology strongly influences the photophysical properties of polyfluorene derivatives.[11,12] Also, the oligomers have been investigated intensely. After optimizing the parameters of length/optical properties, they can also be employed as photonic materials and furthermore they can be used as model compounds to better understand the polymers.[13]

Polyfluorenes show both thermotropic and lyotropic liquid crystalline phases. Liquid crystallinity can be exploited to produce optical anisotropy by orienting films of these materials on a suitable substrate.[14,15] The thermotropic liquid crystalline ordering in polyfluorenes is affected by the nature of the side chains. Grazing incidence X-ray diffraction and electron diffraction measurements on linear and branched alkyl-substituted polyfluorenes have shown that different side chains lead to different molecular arrangements.[16−19] The presence of branched alkyl groups as substituents forces the polyfluorene derivative to adopt a 5_2 helical conformation.[17] In the case of the linear alkyl derivatives, the polymer backbone is found to lie in the plane of the substrate surface, while the spacing between polymer chains normal to the surface depends on the length of the side chains.[18]

Theoretical and computer simulation methods have already given important information about the properties of these materials. Semiempirical and ab initio calculations have been used to characterize their ground-state conformational properties[17,20,21] and their excited states.[22−26] Because these materials are used as functional elements of optoelectronic devices, it is important to study their properties not only as single chains but also in molecular assemblies. The influence of chain interactions on light absorption and emission has been studied by semiempirical calculations on small molecular clusters.[27] More phenomenological models have been employed to simulate the diffusion and relaxation of excitations in thin films by kinetic Monte Carlo algorithms.[28] Finally, molecular mechanics (MM) and molecular dynamics (MD) methods with empirical force fields can also be used.[29] Here the possibility of investigating electronic effects is neglected for computational simplicity, allowing in turn the simulation of much larger systems and an extensive exploration of phase space. The present contribution follows the latter approach because we employ molecular modeling to gain some insight in the conformation and packing of oligofluorenes.

The plan of our manuscript is as follows. In Section II we describe the force field we used in our simulations. Some parameters of the force field, such as the torsional barrier between fluorene units and the nonbonding interactions, were refined in order to have a description of these molecules in agreement with available experimental data. In Section III we test the force field on three different crystalline structures to check the validity of the force field, especially concerning the density and the torsional barrier between two fluorene units. In Section IV we study the presence of different conformational defects and their influence on the molecular packing, including

* Corresponding author. Phone: +39-02-2399-3051, fax: +39-02-2399-3080, e-mail: guido.raos@polimi.it.

[†] Max-Planck-Institut für Polymerforschung.

[‡] Dipartimento di Chimica, Materiali e Ingegneria Chimica "Giulio Natta", Politecnico di Milano.

10.1021/jp056858y CCC: $33.50
Published on Web 03/01/2006

the effect of branched or linear side chains.[17,30,31] In Section V we try to simulate the formation of a ground-state analogue of an excimer-like configuration, which has been linked to the photophysical properties of these materials.[32] Conclusions follow.

II. Force Field Development and ab Initio Calculations

All molecular mechanics and dynamics simulations were performed with the TINKER 4.1 molecular modeling package.[33,34] The force field used in the simulations is based on the MM3 parametrization by Allinger and co-workers.[35] The general strategy adopted to refine it follows previous work by two of us on crystalline oligothiophenes.[36] As a general remark, we stress that conventional force fields (including the present one) do not include polarizability effects, which may be expected to be important in an extensively π-conjugated system. Adopting a pragmatic approach, this enhanced polarizability will be introduced by adjusting the coefficients of the atom−atom dispersion terms ($\propto R^{-6}$) in order to reproduce the experimental crystal structures and, where available, heats of sublimation. Comparison with quantum chemical ab initio calculations provides additional guidance, despite their current limitations in the calculation of nonbonded interactions between large molecules (see below).

The parameters for the intramolecular terms, bonds, angles, and most of the torsions were kept fixed at the original MM3 values. The torsion parameters for the relative rotation between two fluorene units were instead based on ab initio density functional theory (DFT) calculations.[37] The dihedral potential for a fluorene dimer without any side chains was evaluated with the GAMESS-USA program,[38] and it is shown in Figure 1. Molecular geometries were first optimized at the B3LYP/6-311G* level. These were then used in single-point calculations at the B3LYP/6-311++G** level. All of the internal degrees of freedom were optimized, except for the torsional angle, ϕ, that was constrained to 0°, 30°, 60°,..., 180°. Full optimization without any restraints on ϕ were also carried out to determine the positions of the cis-distorted and trans-distorted minima, which are located at 40.8° and 139.7°, respectively (B3LYP/6-311G*). The final dihedral potential is similar to that of biphenyl:[39] it is almost symmetric about the 90° maximum, and the fully planar and orthogonal states have almost exactly the same energy. The relative energies of the equally spaced points were fitted by a six-term Fourier expansion

$$V(\phi) = \sum_{n=0}^{6} a_n \cos\left(\frac{n\pi\phi}{180}\right)$$

where the coefficients have the following values (B3LYP/6-311++G**, in kJ/mol): $a_0 = -4.338$, $a_1 = 0.094$, $a_2 = -0.852$, $a_3 = 0.025$, $a_4 = 4.575$, $a_5 = -0.047$, $a_6 = 0.689$.

It is worth stressing that the intrinsic torsion potential entering a force field is conceptually different from the ab initio one because the latter represents a total energy difference that implicitly includes inter-ring nonbonded interactions, and to a lesser degree also the stretching and bending terms. In particular, within MM3 both electrostatic and van der Waals interactions between 1 and 2 and 1−3 atom pairs (i.e., first and second nearest neighbors) are excluded, whereas 1−4 interactions are fully computed without any rescaling. Therefore, the MM3 intrinsic potential was readjusted with the aim to reproduce the ab initio potential energy curve, after inclusion of all of the other force field terms.

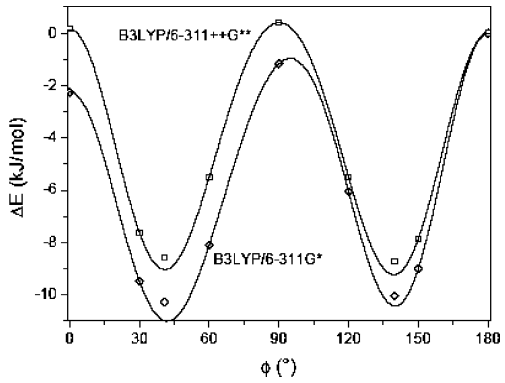

Figure 1. Calculated B3LYP/6-311++G** and B3LYP/6-311G* torsional potential of the fluorene dimer. ϕ is the torsional angle between the two units. The trans planar state corresponds to $\phi = 180°$, and the cis planar corresponds to $\phi = 0°$.

Electrostatic interactions are calculated in the standard MM3 force field as a sum over dipole−dipole interactions. On the basis of our previous experience on oligothiophenes,[36] where we investigated systematically several electrostatic models, we replaced the dipoles with point charges on all atoms. These were obtained by fitting the electrostatic potential produced by the B3LYP electron densities.[40] The values of the charges are given in the Supporting Information.

Van der Waals interactions are represented in the MM3 force field by a Buckingham potential

$$E(r) = \epsilon\left\{-C\left(\frac{r_0}{r}\right)^6 + A\exp\left[-B\left(\frac{r}{r_0}\right)\right]\right\}$$

in which ϵ is the well depth, r_0 is the position of the potential energy minimum, and the other constants have the following values: $A = 184\,000$, $B = 12.0$, $C = 2.25$. Using the standard parameters, the crystal densities obtained from MD simulations at room temperature and atmospheric pressure were 10−20% lower than the experimental values. The same loss of density was also observed in our previous simulations of oligothiophenes.[36] There are at least two possible explanations for this problem. The first one, which has already been stressed above, is that dispersion interactions should be enhanced in these extensively conjugated systems. The second one is that the MM3 parameters were developed especially for simple energy minimizations, rather than room-temperature molecular dynamics or Monte Carlo simulations so that they should be adjusted in the latter case. In any case, we found that a uniform rescaling of all of the interaction energies by increasing the C constant produced the correct densities.[36] Similarly, here we found that we needed to set $C = 3.00$ in order to have good agreement with the experimental crystal structures (see below).

The intermolecular interaction potentials for the models of these systems were also investigated by high-level ab initio calculations. We considered the interaction of three pairs of monomers: two fluorene units, two fluorenone units, and a fluorene with a fluorenone. For each system, we studied two sets of interaction geometries: the two units of these van der Waals complexes were superposed either in a parallel or in an antiparallel fashion, with the carbonyls and/or the methylenes pointing in the same or in opposite directions.

The geometry of the individual units was optimized at the RHF/6-31+G*(0.25) level. We explored the interaction energies as a function of the distance between the molecular centers of mass at the MP2/6-31+G*(0.25) level, without further optimizations. The MP2 method was preferred over DFT methods such

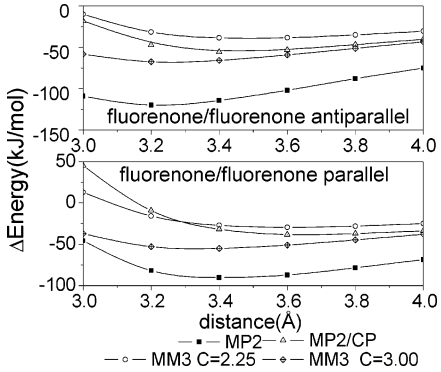

Figure 2. Comparison of ab initio and molecular mechanics potentials for the interaction of two fluorenones.

as B3LYP because the latter do not include dispersion interactions, which are important in these systems.[37,41] The 6-31+G*(0.25) basis set includes a special-purpose set of diffuse *d* functions on second-row elements with an exponent of 0.25. This was developed especially for aromatic intermolecular interactions by Hobza and co-workers.[42] The diffuse polarization functions maximize the dispersion interactions. Calculations of the benzene−benzene interaction energy by Amovilli et al.[43] using similar methods and bases reproduced the results from much more extensive calculations by Tsuzuki et al.[44] (coupled-cluster method with larger basis sets).

Figure 2 compares the ab initio and molecular mechanics potentials for the fluorenone−fluorenone complex in the parallel and antiparallel configurations. There are four curves for each interaction mode: one corresponding to the MP2 calculation, one to MP2 including the cointerpoise (CP) correction for the basis set superposition error (MP2/CP),[41] and two calculated by molecular mechanics, with the *C* parameter equal to 2.25 as in the original MM3 parametrization or to 3.00 as in our modified version. The ab initio well depths decrease by about 50% on going from MP2 to MP2/CP. In addition, the equilibrium distances are affected somewhat, being larger in the latter case. The size of the CP correction can be taken as an indication of the errors that affect ab initio calculations of the interaction between such large molecules using current computational methods. Despite these limitations, MP2/CP may be taken as our ab initio "gold standard". In general, we find that the MP2 method predicts very large interaction energies, while the MP2/CP curve is always bracketed by the molecular mechanics ones with $C = 2.25$ and $C = 3.00$. Similar results were also obtained for the fluorene−fluorene and fluorene−fluorenone complexes. Thus, the ab initio calculations provide further evidence that the MM3 potentials with $C = 2.25$ are probably too weak. However, the present choice of $C = 3.00$ also seems to be too large compared to the MP2/CP data. Nevertheless, we decided to keep this value in the MD simulations to be described below.

Figure 3 contains plots of the MP2/CP potential energy curves for all of the van der Waals complexes. Their interaction energies at the equilibrium geometries are ordered as follows: fluorene−fluorene (less stable) < fluorene−fluorenone < fluorenone−fluorenone (more stable). The equilibrium distances confirm this trend: fluorene−fluorene > fluorene−fluorenone > fluorenone−fluorenone. The fact that fluorenone units can pack more efficiently and interact more strongly than the fluorene units seems to be reasonable, considering that the former are planar whereas the latter are nonplanar because of the presence of an sp^3 carbon. The discrimination between the parallel and antiparallel configurations is also interesting. In all cases, the antiparallel configuration is more stable. The energetic

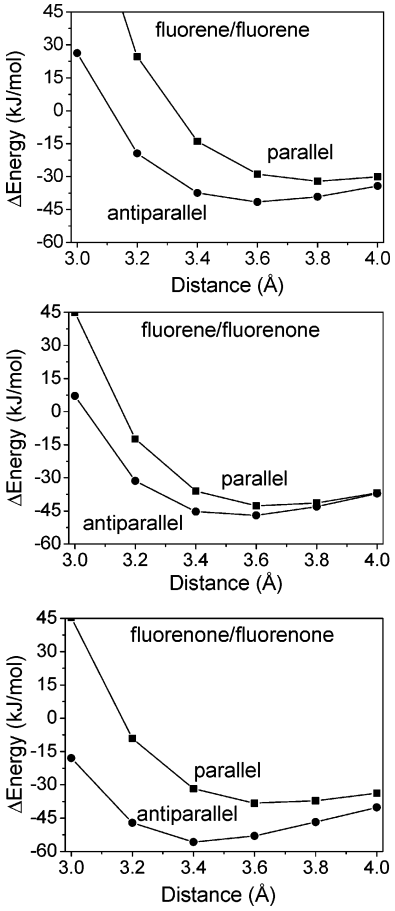

Figure 3. Ab initio potentials (MP2/CP) for the interaction of fluorene and fluorenone units in parallel and antiparallel configurations.

difference is largest in the fluorenone−fluorenone complex (about 18 kJ/mol), and this is most likely due to the electrostatic interaction between the carbonyl dipoles. The parallel configuration of the fluorene−fluorene complex is destabilized over the parallel one by about 12 kJ/mol. Now the main mechanism for the discrimination is probably the steric repulsion between the methylene groups. Finally, there is almost no discrimination in the fluorene−fluorenone complex because in this case the parallel and antiparallel minima are found at very similar distances and their energies differ by less than 4 kJ/mol.

III. Simulation of Model Crystal Structures

Our force field was tested on three different crystal structures[45] that contained fluorene and fluorenone units as shown in Figure 4. All of the systems have ethyl-hexyl side chains, which contain a chiral carbon. The molecules were synthesized from a racemic mixture. This is the main reason for the large disorder in the crystal structures, especially concerning the fractional coordinates of the side chains. We performed "constant pressure−temperature" (NPT for short) molecular dynamics simulations at $T = 300$ K and $P = 1.0$ atm, which were controlled by the Berendsen method[46] (the coupling times are 0.2 ps for the pressure and 2.0 ps for the temperature). We implemented within TINKER the Berendsen coupling for anisotropic triclinic systems to perform simulations with a variable box shape. The cutoff for the electrostatic and van der Waals interactions was fixed at the default value of 9.5 Å.

The molecule of the first crystal structure (**1**) is a fluorene monomer capped with two five-membered rings containing a boron, two oxygens, and two carbons (see Figure 4). The cell

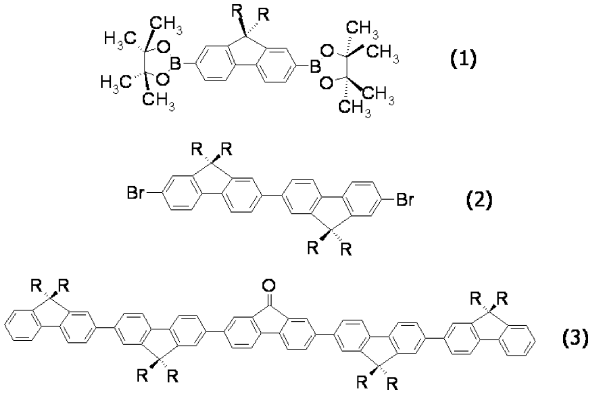

Figure 4. Schemes of the molecule of the three crystal structures. The side chains are always ethyl-hexyl in the experimental crystal cells. Octyl side chains were also considered in some simulations.

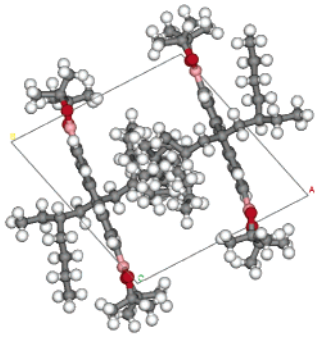

Figure 5. Unit cell of molecule **1**. The space group is $P\bar{1}$.

TABLE 1: Molecular Dynamics Results for the Crystal Structure of 1

lattice	experiment	MD NPT	deviation (%)
a (Å)	12.533	12.466	−0.5%
b (Å)	13.117	12.977	−1.0%
c (Å)	13.171	13.310	+1.0%
α	108.196	108.84	+0.6%
β	92.625	92.31	−0.3%
γ	102.320	101.33	−1.0%
density (g/cm^3)	1.058	1.078	+1.8%

is shown in Figure 5. The spacegroup is $P\bar{1}$. The results of the NPT simulations are in Table 1, which contains the average density as well as the cell axes and angles. The simulated values are in good agreement with the experimental data. Figure 6 shows the root-mean-square deviation (RMSD) of the atoms from the crystallographic coordinates. The RMSD of the backbone is around 0.01 nm, showing that during the simulation it stays very close to the experimental position. The RMSD of the two terminal rings is of the order of 0.02 nm. This value increases up to 0.03−0.04 nm with the inclusion of the methyl groups, as expected because of the higher freedom of these groups.

The second crystal structure, which is shown in Figure 7, is based on a fluorene dimer with two bromines as terminal atoms (**2**). The space group of the cell is $P\bar{1}$. The results of the simulation are in Table 2. The deviation from experiment of the simulated values is higher than in the case of **1**. This is most likely due to the incomplete refinement of the starting crystal structure and the high disorder of the side chains. We also analyzed the value of the torsional angle between the two fluorene units of the dimers in order to check that the dihedral potential derived from ab initio gas-phase calculations reproduces the conformational behavior of these molecules in the solid state. The distribution of these dihedrals during the MD

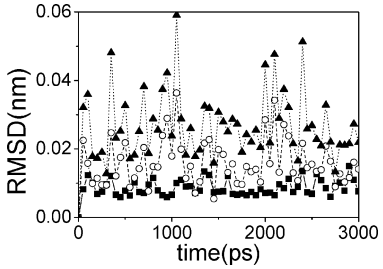

Figure 6. Root-mean-square deviation from crystallographic coordinates in the MD simulation of the crystal of **1**. The −■− line refers to the atoms belonging to the fluorene monomer. The other lines refer to the terminal five-membered rings, excluding (−○−) or including (−▲−) the methyl groups.

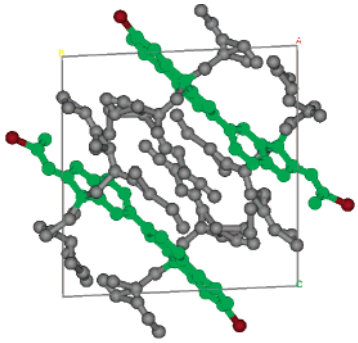

Figure 7. Experimental unit cell of molecule **2**. The fluorene backbone is green, and the side chains are gray.

TABLE 2: Molecular Dynamics Results for the Crystal Structure of 2

lattice	experiment	MD NPT	deviation (%)
a (Å)	13.086	14.059	+7.4%
b (Å)	13.865	13.764	−0.7%
c (Å)	15.072	14.689	−2.5%
α	85.607	79.36	−7.2%
β	71.699	68.03	−5.1%
γ	83.829	80.86	−3.6%
density (g/cm^3)	1.187	1.204	+1.4%

run at 300 K, shown in Figure 8, is centered at 145°, in excellent agreement with the experimental value of 145.3°.

The third crystal structure,[45] shown in Figure 9, is based on a fluorene pentamer with a fluorenone unit at the center (**3**). The space group of this cell is $P2_1/c$. The results of the simulation are in Table 3 and show good agreement with the experimental data. The presence of branched alkyl side chains forces oligo- and polyfluorenes to adopt the 5_2 helical conformation.[17,47] The experimental values for the torsional angles of the present pentamer are +141.7°, +137.4°, −156.5°, and +36°. Thus, it also adopts a 5_2 helical conformation, but with a reversed angle in the proximity of the fluorenone group and a cis conformation at one end. Figure 10 shows the inclination angle between the units in the pentamer. This angle represents

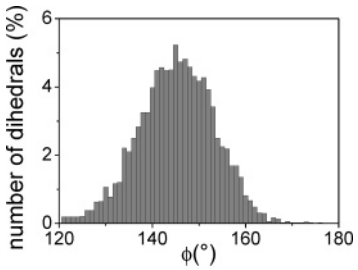

Figure 8. Histogram of the torsional angles between the two fluorene units during the MD simulation of the crystal structure of **2**.

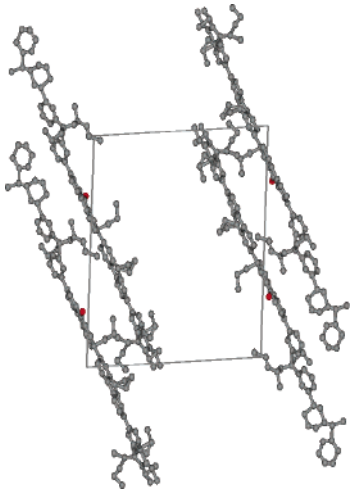

Figure 9. Experimental unit cell of molecule **3**. Note that the side chains are only partially resolved.

TABLE 3: Molecular Dynamics Results for the Crystal Structure of Molecule 3

lattice	experiment	MD NPT	deviation (%)
a (Å)	23.396	23.784	+1.7%
b (Å)	19.066	19.061	+2.8%
c (Å)	24.324	23.414	−3.7%
β	94.898	99.32	+4.7%
density (g/cm^3)	1.054	1.063	+0.9%

the deviation from planarity of two directly connected units, discarding differences between $+\phi$ and $-\phi$ values (the absolute value is considered) and between cis and trans conformations (for the latter we take $180° - \phi$). The average inclination angle is around 35°, in agreement with the 5_2 helix-like conformation, where, with a dihedral angle of 144°, there is an inclination angle of 36°.

IV. Main- and Side-Chain Conformation

Having established the reliability of our force field for modeling crystalline fluorenes, we have used it to investigate some geometric and energetic aspects connected to molecular packing and conformation. The conformational behavior of the fluorene backbone has been investigated mainly in the case of solutions.[17,48] These studies have already established that the structure of the side chains has a significant impact on the conformation of the conjugated backbone. Oligofluorene thin films are often generated by spin-coating, a process that produces amorphous or polycrystalline materials and in which there is little control on the conformational and positional order. In particular, helix reversals are believed to have a significant impact on the optical and electronic properties of these materials because any conformational defect destroys the continuity of the π system, produces a distribution of conjugation lengths, and increases the energetic disorder of the electronic levels. Therefore, it is pertinent to ask whether and how helix reversals may also become possible within bulk phases, including crystals.

IV.1. Influence of Different Side Chains. The effect of the side chains on the conformation of oligofluorene pentamer **3** was investigated by considering both the branched ethyl-hexyl and the linear octyl cases. Although there is no doubt that branched alkyl side chains force poly- and oligofluorenes to adopt the 5_2 helical conformation,[17,47] the conformational behavior of the backbone in the presence of octyl side chains is still a subject of debate. Nonetheless, it is generally agreed that in this case the polymeric backbone is more planar, leading

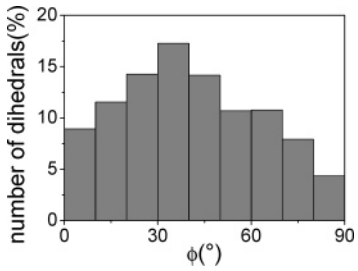

Figure 10. Histogram of the inclination angle between the planes of the aromatic rings from the MD simulation of the crystal of **3**.

TABLE 4: Average Energies and Errors (in kJ/mol) from the MD Simulations of Molecule 3 in Vacuo at 300 K, with Either Octyl or Ethyl-Hexyl Side Chains[a]

	RRLL	RLRL	planar	planar-175°
octyl	−6.590 (±6.187)	1.485 (±5.543)	26.492 (±5.558)	2.030 (±5.575)
ethyl-hexyl	0.881 (±4.636)	−1.039 (±4.652)	41.021 (±4.580)	43.819 (±4.602)

[a] The average RRRR energy is 0 kJ/mol by definition, having been taken as the reference value.

to a much longer effective conjugation length than that observed in the molecules with branched side chains.[16] Further measurements on the conformational behavior[18,31,49,50] and investigations on the impact of this more planar structure on the photophysical properties[49,51] have also been reported.

We first performed gas-phase MD simulations at 300 K. Such simulations ignore the steric requirements produced by neighboring chains in crystals, which will be addressed afterward. We constrained the chain backbone to adopt five different conformations:

RRRR Conformation. All torsions are fixed at +144°. This corresponds to the conformation of an ideal 5_2 helix. We use this conformation as reference, to compute the relative energy of the other ones.

RRLL Conformation. The torsions are fixed at 144°, 144°, −144 °, and −144°. There is an inversion from right-handed to left-handed in the middle of the chain.

RLRL Conformation. The torsional angles are +144°, −144°, +144°, and −144°. Assuming this to be a part of a longer ...RRRLRLLL... sequence, the net result is again an inversion from right-handed to left-handed. Alternatively, this may also be seen as a model for a long nonhelical ...RLRLRLRL... sequence.

Planar Conformation. All of the torsional angles are constrained to be perfectly planar, at 180°.

Planar-175 Conformation. All torsions are constrained to be nearly planar, at +175°.

The constraints were applied in the form of additional steep harmonic potentials acting on the main-chain torsional angles. This leaves the side chains free to move about their minimum-energy states.

The average energies relative to the RRRR reference are given in Table 4. For the pentamer with ethyl-hexyl side chains, we can see that both the planar and planar-175 conformations are much higher in energy than the three helix-like conformations, which are within 1−2 kJ/mol from each other. In the octyl case the conformation with minimum energy is RRLL, followed by RRRR and RLRL. The planar conformation has again a very high energy, whereas the planar-175 state is now much closer to the three helix-like conformations. The high value of the planar conformation can be explained by the steric hindrance of the hydrogens in the fluorene units: according to the ab initio

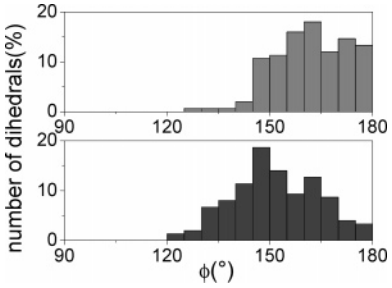

Figure 11. Histograms of the torsional angles between the two fluorene units, from a simulation of a dimer in vacuo. The upper graph refers to the case of octyl side chains; the lower one refers to the case of ethyl-hexyl side chains.

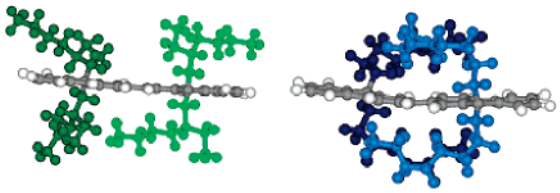

Figure 12. Representative snapshots from the simulations of dimers in vacuo. On the left side is the case with ethyl-hexyl side chains, and on the right side is the case with octyl side chains. Note that the main-chain torsional angle is about 180° in both cases.

potential, the 0° and 180° states are also very unfavorable without any substituents. This steric repulsion is surely also present in the slightly distorted planar-175 conformation. However, it is largely compensated by a favorable interaction between the linear side chains.

The importance of the structure of the alkyl substituents is confirmed by the histograms of torsional angles in Figure 11. These were obtained from 2-ns MD simulations at 300 K of a fluorene dimer in vacuo (**2**, without Br terminals), with either ethyl-hexyl or octyl side chains. The lower graph shows that the distribution is centered around 145° in the ethyl-hexyl case, as expected. In the case of the octyl side chains (upper graph), we observe a shift in the dihedral distribution toward a more planar conformation. Snapshots from the dynamics clearly show that the linear side chains are forming comfortable contacts in this case (Figure 12).

We have also simulated the conformational behavior in bulk in order to study the effect of intermolecular interactions. For each type of side chain, we built a simulation box containing eight pentamers without keto-defects. In the initial configuration the pentamers have an all RRRR conformation, but the torsion angles, during the simulation, are not constrained. We performed an NPT simulation at 300 K and 1 atm to equilibrate the system. At the beginning, the system has a very low density. The density increases during the simulation because of nonbonded interactions between the pentamers inside the box until an equilibrium value is reached (0.992 g/cm^3 and 1.096 g/cm^3, respectively, for ethyl-hexyl and octyl). The system is moving from a very diluted configuration to a condensed state. It is important to point out that in the simulation this process is faster than in a physical system, where the aggregation process has a time scale of seconds. We then ran "constant volume−temperature" (NVT) simulations for 2 ns to obtain the two dihedral distributions shown in Figure 13. We see that the high population of near-planar conformations for the oligomers with octyl side chains has largely disappeared on going from the gas to the bulk phase, but instead there is a high percentage (more than 50%) of dihedrals with a cis conformation. The cis population is not very significant in the case of the ethyl-hexyl side chains, where

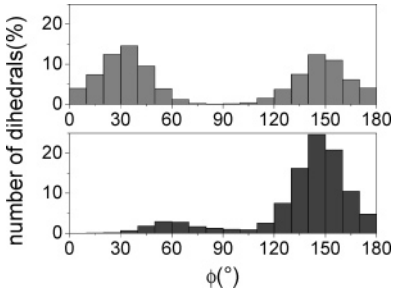

Figure 13. Histograms of the torsional angles between the units of fluorene pentamers, obtained from the MD simulations in bulk. The upper graph refers to the case of octyl side chains, and the lower one refers to the case of ethyl-hexyl side chains.

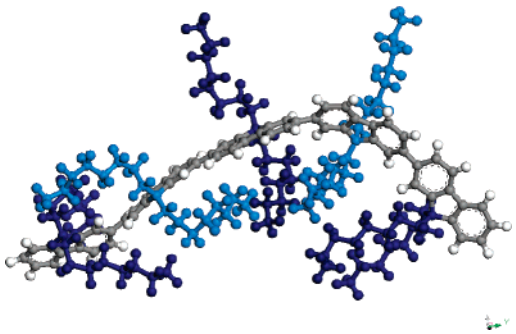

Figure 14. Representative snapshot of a single molecule, from the bulk simulation of the pentamers with octyl side chains.

the most likely dihedrals remain close to 145°. The presence of so many cis conformations in the bulk octyl case can be explained by examining some snapshots of the simulations closely (Figure 14), where it can be seen that the cis dihedrals favor the interactions of side chains belonging to two connected units of the same molecule. This effect is less important in the case of the ethyl-hexyl chains.

We also characterized the orientational order of the molecules through the nematic order parameter

$$\langle P_2 \rangle = \left\langle \frac{3}{2}\cos^2\theta - \frac{1}{2} \right\rangle$$

where θ is the angle formed by the instantaneous vector of a molecule (connecting the terminal carbon atoms on the first and fifth fluorene units) and the average direction of this vector in the same frame, and the angular brackets $\langle \bullet \rangle$ denote an average over time and over all molecules of the simulation box. The values of $\langle P_2 \rangle$ are 0.77 and 0.45, respectively, for the branched and the linear side chains. These values show a greater tendency of the pentamers with branched side chains to adopt a more orientationally ordered state. We also evaluated the average head-to-tail distance for the two types of molecules. This distance is 38.0 Å (±2.1 Å) for the ethyl-hexyl case and 34.2 Å (±5.0 Å) for the octyl case. These differences in length contraction and shape fluctuation correlate well with the population of torsional states and lower orientational order discussed previously.

IV.2. Conformational Defects within the Crystals. The previous results show that the helix reversals are certainly possible in solution and in the liquid-crystalline state. In the solid state, however, there are stronger energetic and steric requirements on a helix inversion because this must be compatible with the constraints imposed by the crystal cell. Using the crystals of pentamer **3** with the keto-defect and ethyl-hexyl side chains as a model, we have investigated this problem considering

TABLE 5: MD Results for the Crystals of Molecule 3 with Constrained Conformations on the Four Chains within the Unit Cell[a]

	a axis (Å)	*b* axis (Å)	*c* axis (Å)	β (deg)	density (g/cm^3)
RRLL	23.076	19.519	24.304	101.83	1.072
	(−1.37%)	(−2.37%)	(−0.08%)	(+7.34%)	(+1.69%)
RLRL	19.327	23.255	23.566	93.46	1.073
	(−17.39%)	(−23.55%)	(−3.12%)	(−1.52%)	(+1.76%)
planar	24.108	18.902	24.311	99.41	1.049
	(+3.04%)	(−0.86%)	(−0.05%)	(+4.75%)	(−0.47%)

[a] The deviations from the experimental data are shown in brackets. Analogous data for the reference RRRR state have been given in Table 3.

TABLE 6: MD Results for the Crystal Structure of Molecule 3 with Different Constrained Conformations on One out of the Four Chains Present in the Unit Cell[a]

	density (g/cm^3)	*F*
RRRL (+ + + −)	1.042 (−1.17%)	125.93
RRLR (+ + − +)	1.055 (+0.07%)	385.85
RRLL (+ + − −)	1.032 (−2.06%)	200.43
RLLR (+ − − +)	1.046 (−0.76%)	198.86
RLRL (+ − + −)	1.029 (−2.34%)	112.83
RLLL (+ − − −)	1.028 (−2.46%)	447.40
planar	1.020 (−3.23%)	188.268

[a] Parameter *F* measures the deviation of the cell lengths and angles from the experimental data.

both collective and single-chain reversals (simultaneous inversion of all helices or of a single helix within the unit cell).

The collective reversals were modeled by forcing all four molecules in the cell to adopt the same conformation. We studied three different cases: the RRLL conformation (+144° +144° −144° −144°), the RLRL conformation (+144° −144° +144° −144°), and the fully planar conformation with all of the dihedral angles fixed at 180°. We performed NPT simulations at 300 K and 1 atm, and we analyzed the deviations of the axes, angles, and density from the experimental defect-free cell. As can be seen from Table 5, the density is only slightly affected by the conformational defects. Also, the individual cell parameters remain close to the experimental data in the case of the RRLL and planar conformations. Instead, the RLRL conformation produced extremely high distortions of the *a* and *b* axes. Therefore, this specific mode of collective helix reversal seems to be incompatible with the crystal packing, unlike the two former ones.

Similar NPT simulations at 300 K and 1 atm were used to investigate the behavior of single-chain inversions within the crystal (one helix reversal out of four chains within the unit cell). Table 6 provides the overall density and a structural parameter, *F*, which summarizes the distortions of the unit-cell lengths and angles[52]

$$F = (100\Delta a/a)^2 + (100\Delta b/b)^2 + (100\Delta c/c)^2 + \Delta\alpha^2 + \Delta\beta^2 + \Delta\gamma^2$$

The density of all of the simulated crystals are comparable to the experimental values. The defect that is most compatible with the crystal structure is the one having the RLRL conformation, having the lowest value of the structural factor, *F*.

To summarize, both collective and single-chain reversals appear to be possible, or at least compatible with the constraints of crystalline packing. The most likely conformational defects leading to inversion appear to be RRLL or planar in the first case and RLRL in the second case.

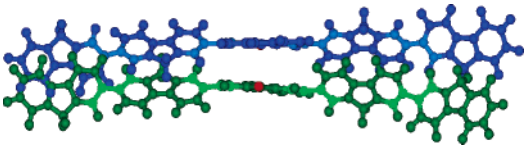

Figure 15. Figure of the configuration of two pentamers investigated as a model of an excimer precursor. The interfluorene torsions have been highlighted using brighter colors.

V. Possibility of an Excimer-Like Conformation

Because oligo- and poly-fluorenes are blue emitters in the field of organic-based displays, their spectral purity is a major issue for further improvement. Unfortunately, an unwanted broad red-shifted emission band ("green band") appears in the presence of air. The origin of this emission has been debated by several authors.[12,45,53−64] Two alternative interpretations have been proposed: (a) formation of keto-defects on the backbone due to a photooxidative process so that the carbonyl groups can then act as low-energy traps for electrons or (b) intermolecular aggregation of the chain backbones so that the resulting aggregates may also trap the electronic excitations and relax through excimers (see, for example, ref 57). As a consequence, supporters of (a) have emphasized the need to work with chemically very pure samples in order to avoid the green emission (see, for example, ref 3), whereas proponents of (b) have proposed the use of bulky side groups in order to avoid aggregation. Recent work has clearly proven that the pronounced green emission in electroluminescence experiments is due to preferential trapping of electrons on the keto defects.[61,64]

We have used our molecular modeling tools to investigate the possible formation of a ground-state precursor of an excimer. The geometrical configuration that can lead to an excimer after optical excitation consists of two fluorene or two fluorenone units, face-to-face and parallel to each other like the two central units in Figure 15. This shows two **3** pentamers in which all of the side chains have been replaced by hydrogens. This was done to model the system under the most favorable conditions, avoiding any interference due to the steric hindrance of alkyl groups.

We took as a starting point the unit cell of the pentamer. The side chains were deleted, and two out of four molecules were moved to form the excimer-like configuration shown in Figure 15. The system's volume was adjusted by a short NPT simulation. We then performed three sets of energy minimizations using different combinations of constraints on the dihedral angles next to the central units of these two molecules:

Case 1. Only one dihedral angle in one of the molecule is constrained

Case 2. Both dihedrals next to the central unit of one molecule are constrained

Case 3. The two dihedrals next to fluorenone unit are constrained in both molecules.

For each of the three cases, the central C═O groups can be either parallel or antiparallel.

Figure 16 shows the results only for the antiparallel carbonyls, those for the parallel case being very similar. Also, the three strategies used to constrain the central torsions lead to identical conclusions. The distance between the two central fluorenones (upper graph) and the angle formed by the vectors normal to these units (lower graph) have been plotted as a function of the constrained dihedral(s). When the conformation at the central units tends toward coplanarity, the distance between their centers of mass decreases to about 3.25 Å, but the orientation angle

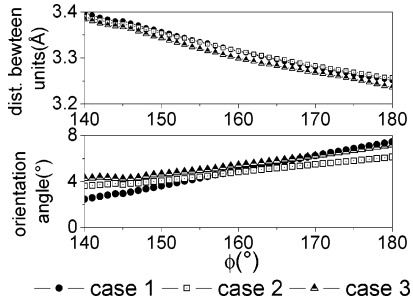

Figure 16. Results of the minimization for an excimer-like conformation. The *x* axis indicates the dihedral angle of the chains (further explanation in the text). The *y* axis in the upper graph corresponds to the distance between the centers of mass of the two central units. The *y* axis of the lower graph corresponds to the angle between the normal vectors of the two units.

TABLE 7: Results of the Minimization for an Excimer-Like Conformation without Any Restraint on the Chains[a]

	unit 1	unit 2	unit 3	unit 4	unit 5
orientation (deg)	5.02	13.29	25.19	21.21	6.45
distance (Å)	4.04	5.95	3.85	4.99	8.64
orientation (deg)	5.77	7.68	13.77	24.79	24.89
distance (Å)	3.54	4.03	3.54	5.22	8.73

[a]The first two lines of the table refer to the parallel case, and the last two lines refer to the antiparallel case.

between the units increases. This means that when the units get closer the deviation from the parallel configuration increases.

We also performed two minimizations, one for the parallel configuration of the C═O bonds and one for the antiparallel case, without any constraints on the dihedral angles. The results are shown in Table 7. They demonstrate once more the tendency of the two central units not to be perfectly parallel, adopting instead the herringbone-like configuration typical of aromatic crystals. Also, the equilibrium distance between the units is always much larger than the value predicted by the force-field and ab initio calculations on the isolated units (≅3.2−3.4 Å, see the fluorenone/fluorenone case in Figure 3). Furthermore, the distance between the end units of the pentamers is considerably larger, showing that the two molecules tend to move apart and their helix-like conformations are destroyed. Finally, we calculated the energy related to the unperturbed crystal (−374.6 kcal/mol) and the energies of the crystals having two molecules in the excimer-like conformation (−350.6 kcal/mol in the parallel case and −355.4 kcal/mol in the antiparallel case). The formation of an excimer precursor also seems to be unlikely from an energetic point of view.

VI. Conclusions

We have presented a molecular modeling study of oligofluorenes. First of all, we have presented the results of ab initio calculations and we have developed a force field that is capable of describing these systems. We tested its validity by room-temperature molecular dynamics simulations of three different crystal structures. The force field, based on MM3, was modified for what concerns the torsional barrier between two fluorene units and the electrostatic interactions. We derived both the torsional potential and the point charges from ab initio calculations. We also found that the standard MM3 exp-6 parameters lead to crystal densities that are too low (typically by ≅10−20%). Similar to a previous study on oligothiophenes, this forced us to modify the van der Waals parameters, increasing homogeneously all C_6 dispersion coefficients. High-level ab initio calculations (MP2 with a moderately large basis set) of the interaction energies between fluorene and fluorenone monomers have provided some additional support for this empirical procedure.

We have employed this force field and MD simulations to investigate the influence of different side chains on the conformation of the conjugated backbone. We have considered the cases of branched or linear side chains. With ethyl-hexyl side chains, the oligomers adopt the well-known 5_2 helix-like conformation. The presence of octyl side chains allow the backbone to adopt a more planar configuration when a single chain in vacuo is considered. However, this effect is reduced in bulk because of the stronger interactions between the linear side chains.

We have also studied the possibility of accommodating different helix reversals from right-handed (R) to left-handed (L) in the crystal structure of a helical pentamer. We found that all of the molecules in the unit cell can have an RRLL or a planar conformation, without disturbing the crystal, whereas the RLRL conformation leads to great distortions in the molecular packing. This conformation is instead the most likely defect that a crystal structure can host when only a molecule has a conformation different from the all-R one.

Finally, we considered the possibility of having an excimer-like configuration inside a crystal-like environment. In this configuration, two fluorenone units are parallel to each other and face-to-face. We considered the fluorenone units because the keto defects seem to be responsible for the presence of an additional green emission. From our calculations it appears that the formation of an excimer precursor in the ground state seems to be unlikely from both a geometrical and an energetic point of view, in agreement with recent reports by one of us[45] and others.

Acknowledgment. We thank Dr. V. Enkelmann for providing the crystal structures and Dr. C. Chi for useful discussions. Dr. P. Kevainidis deserves special thanks for his help and support. V. M. acknowledges the IMPRS (International Max Planck Research School) for financial support. G. R. thanks the MIUR-PRIN2004 program for support.

Supporting Information Available: Ab initio atomic charges entering the force field. This material is available free of charge via the Internet at http://pubs.acs.org.

References and Notes

(1) Leclerc, M. *J. Polym. Sci., Part A* **2001**, *39*, 2867−2873.
(2) Neher, D. *Macromol. Rapid Commun.* **2001**, *22*, 1365−1385.
(3) Scherf, U.; List, E. J. W. *Adv. Mater.* **2002**, *14*, 477−487.
(4) Bernius, M. T.; Inbasekaran, M.; O'Brien, J.; Wu, W. S. *Adv. Mater.* **2000**, *12*, 1737−1750.
(5) Halls, J. J. M.; Arias, A. C.; Mackenzie, J. D.; Wu, W. S.; Insbasekaran, M.; Woo, E. P.; Friend, R. H. *Adv. Mater.* **2000**, *12*, 498−502.
(6) Virgili, T.; Lidzey, D. G.; Bradley, D. D. C. *Adv. Mater.* **2000**, *12*, 58−62.
(7) Laquai, F.; Im, C.; Kadashchuk, A.; Bässler, H. *Chem. Phys. Lett.* **2003**, *375*, 286−291.
(8) Li, B.; Li, J. L.; Fu, Y.; Bo, Z. *J. Am. Chem. Soc.* **2004**, *126*, 3430−3431.
(9) Charas, A.; Morgado, J.; Martinho, J. M. G.; Alcácer, L.; Cacialli, F. *Chem. Commun.* **2001**, *13*, 1216−1217.
(10) Chen, X.; Liao, J.-L.; Liang, Y.; Ahmed, M. O.; Tseng, H.-E.; Chen, S.-A. *J. Am. Chem. Soc.* **2003**, *125*, 636−637.
(11) Ariu, M.; Lidzey, D. G.; Sims, M.; Cadby, A. J.; Lane, P. A.; Bradley, D. D. C. *J. Phys. Condens. Matter* **2002**, *14*, 9975−9986.
(12) Sainova, D.; Neher, D.; Dobruchowska, E.; Luszczynska, B.; Glowacki, I.; Ulanski, J.; Nothofer, H.-G.; Scherf, U. *Chem. Phys. Lett.* **2003**, *371*, 15−22.
(13) Mullen, K.; Wegner, G. *Electronic Materials: The Oligomer Approach*; Wiley-VCH: New York, 1998.

(14) Grell, M.; Bradley, D. D. C.; Inbasekaran, M.; Woo, E. P. *Adv. Mater*. **1997**, *9*, 798−802.
(15) Sainova, D.; Zen, A.; Nothofer, H. G.; Asawapirom, U.; Scherf, U.; Hagen, R.; Bieringer, T.; Kostromine, S.; Neher, D. *Adv. Funct. Mater*. **2002**, *12*, 49−57.
(16) Grell, M.; Bradley, D. D. C.; Ungar, G.; Hill, J.; Whitehead, K. S. *Macromolecules* **1999**, *32*, 5810−5817.
(17) Lieser, G.; Oda, M.; Miteva, T.; Meisel, A.; Nothofer, H. G.; Scherf, U.; Neher, D. *Macromolecules* **2000**, *33*, 4490−4495.
(18) Kawana, S.; Durrell, M.; Lu, J.; MacDonald, J. E.; Grell, M.; Bradley, D. D. C.; Jukes, P. C.; Jones, R. A. L.; Bennett, S. L. *Polymer* **2002**, *43*, 1907−1913.
(19) Knaapila, M.; Lyons, B. L.; Kisko, K.; Foreman, J. P.; Vainio, U.; Mihaylova, M.; Seeck, O. H.; Lars-Olof, P.; Serimaa, R.; Torkkeli, M.; Monkman, A. P. *J. Phys. Chem. B* **2003**, *107*, 12425−12430.
(20) Belletete, M.; Ranger, M.; Beaupré, S.; Leclerc, M.; Durocher, G. *Chem. Phys. Lett.* **2000**, *316*, 101−107.
(21) Pan, J.-F.; Hou, X.-Y.; Chua, S.-J.; Huang, W. *Phys. Chem. Chem. Phys*. **2002**, *4*, 3959−3964.
(22) Oda, M.; Nothofer, H.-G.; Scherf, U.; Šunjić, V.; Richter, D.; Regenstein, W.; Neher, D. *Macromolecules* **2002**, *35*, 6792−6798.
(23) Tirapattur, S.; Belletete, M.; Leclerc, M.; Durocher, G. *J. Mol. Struct.: THEOCHEM* **2003**, *625*, 141−148.
(24) Franco, I.; Tretiak, S. *Chem. Phys. Lett*. **2003**, *372*, 403−408.
(25) Wang, J.-F.; Feng, J.-K.; Ren, A.-M.; Liu, X.-D.; Ma, Y.-G.; Lu, P.; Zhang, H.-X. *Macromolecules* **2004**, *37*, 3451−3458.
(26) Brière, J.-F.; Côté, M. *J. Phys. Chem. B* **2004**, *108*, 3123−3129.
(27) Cornil, J.; Beljonne, D.; Calbert, J.-P.; Brédas, J.-L. *Adv. Mater*. **2001**, *13*, 1053−1067.
(28) Meskers, S. C. J.; Hübner, J.; Oestreich, M.; Bässler, H. *Chem. Phys. Lett.* **2001**, *339*, 223−228.
(29) Leclère, Ph.; Hennebicq, E.; Calderone, A.; Brocorens, P.; Grimsdale, A. C.; Müllen, K.; Brédas, J.-L.; Lazzaroni, R. *Prog. Polym. Sci*. **2003**, *28*, 55−81.
(30) Chunwaschirasiri, W.; Tanto, B.; Huber, D. L.; Winokur, M. J. *Phys. Rev. Lett.* **2005**, *94*, 107402.
(31) Chen, S. H.; Chou, H. L.; Su, A. C.; Chen, S. A. *Macromolecules* **2004**, *37*, 6833−6838.
(32) Jenekhe, S. A.; Osaheni, J. A. *Science* **1994**, *265*, 765−768.
(33) Ponder, J. W. *TINKER: Software Tools for Molecular Design*, 4.1 ed.; Washington University School of Medicine: Saint Louis, MO, 2003.
(34) (a) Ren, P.; Ponder, J. W. *J. Comput. Chem.* **2002**, *23*, 1497−1506. (b) Ren, P.; Ponder, J. W. *J. Phys. Chem. B* **2003**, *107*, 5933−5947. (c) Pappu, R. V.; Hart, R. K.; Ponder, J. W. *J. Phys. Chem. B* **1998**, *102*, 9725−9742. (d) Hodsdon, M. E.; Ponder, J. W.; Cistola, D. P. *J. Mol. Biol.* **1996**, *264*, 585−602. (e) Kundrot, C. E.; Ponder, J. W.; Richards, F. M. *J. Comput. Chem.* **1991**, *12*, 402−409. (f) Ponder, J. W.; Richards, F. M. *J. Comput. Chem.* **1987**, *8*, 1016−1024.
(35) (a) Allinger, N. L.; Yuh, Y. H.; Li, J.-H. *J. Am. Chem. Soc.* **1989**, *111*, 8551−8566. (b) Li, J.-H.; Allinger, N. L. *J. Am. Chem. Soc.* **1989**, *111*, 8566−8575 and 8576−8582.
(36) Marcon, V.; Raos, G. *J. Phys. Chem. B* **2004**, *108*, 18053−18064.
(37) Koch, W.; Holthausen, M. C. *A Chemist's Guide to Density Functional Theory*; Wiley-VCH: Weinheim, Germany, 2000.
(38) Schmidt, M. W.; Baldridge, K. K.; Boatz, J. A.; Elbert, S. T.; Gordon, M. S.; Jensen, J. H.; Koseki, S.; Matsunaga, N.; Nguyen, K. A.; Su, S. J.; Windus, T. L.; Dupuis, M.; Montgomery, J. A. *J. Comput. Chem.* **1993**, *14*, 1347−1363.
(39) Cacelli, I.; Prampolini, G. *J. Phys. Chem. A* **2003**, *107*, 8665−8670.
(40) Spackman, M. A. *J. Comput. Chem*. **1996**, *17*, 1−18.
(41) Stone, A. J. *The Theory of Intermolecular Forces*; Oxford University Press: Oxford, 1996.
(42) Hobza, P.; Selzle, H. L.; Schlag, E. W *J. Phys. Chem*. **1996**, *100*, 18790−18794.
(43) Amovilli, C.; Cacelli, I.; Campanile, S.; Prampolini, G. *J. Chem. Phys*. **2002**, *117*, 3003−3012.
(44) Tsuzuki, S.; Honda, K.; Uchimaru, T.; Mikami, M.; Tanabe, K. *J. Am. Chem. Soc*. **2002**, *124*, 104−112.
(45) Chi, C.; Im, C.; Enkelmann, V.; Ziegler, A.; Lieser, G.; Wegner, G. *Chem.*−*Eur. J.* **2005**, *11*, 6833−6845.
(46) Berendsen, H. J. C.; Postma, J. P. M.; van Gunsteren, W. F.; DiNola, A.; Haak, J. R. *J. Chem. Phys.* **1984**, *81*, 3684−3690.
(47) Fytas, G.; Nothofer, H. G.; Scherf, U.; Vlassopoulos, D.; Meier, G. *Macromolecules* **2002**, *35*, 481−488.
(48) Wu, L.; Sato, T.; Tang, H.; Fujiki, M. *Macromolecules* **2004**, *37*, 6183−6188.
(49) Winokur, M. J.; Slinker, J.; Huber, D. L. *Phys. Rev. B*, **2003**, *67*, 184106.
(50) Ariu, M.; Lidzey, D. G.; Lavrentiev, M.; Bradley, D. D. C.; Jandke, M.; Strohriegl, P. *Synth. Met.* **2001**, *116*, 217−221.
(51) Ariu, M.; Sims, M.; Rahn, M. D.; Hill, J.; Fox, A. M.; Lidzey, D. G.; Oda, M.; Cabanillas-Gonzalez, J.; Bradley, D. D. C. *Phys. Rev. B* **2003**, *67*, 195333.
(52) Filippini, G.; Gavezzotti, A. *Acta Crystallogr*. **1993**, *B 49*, 868−880.
(53) Yan, M.; Rothberg, L. J.; Papadimitrakopoulos, F.; Galvin, M. E.; Miller, T. M. *Phys. Rev. Lett.* **1994**, *73*, 744−747.
(54) Antoniadis, H.; Rothberg, L. J.; Papadimitrakopoulos, F.; Yan, M.; Galvin, M. E.; Abkowitz, M. A. *Phys. Rev. B* **1994**, *50*, 14911−14915.
(55) Rothberg, L. J.; Yan, M.; Papadimitrakopoulos, F.; Galvin, M. E.; Kwock, E. W.; Miller, T. M. *Synth. Met.* **1996**, *80*, 41−58.
(56) Kreyenschmidt, M.; Klaerner, G.; Fuhrer, T.; Ashenhurst, J.; Karg, S.; Chen, W. D.; Lee , V. Y.; Scott, J. C.; Miller, R. D *Macromolecules* **1998**, *31*, 1099−1103.
(57) Bliznyuk, V. N.; Carter, S. A.; Scott, J. C.; Klärner, G.; Miller, R. D.; Miller, D. C. *Macromolecules* **1999**, *32*, 361−369.
(58) List, E. J. W.; Guentner, R.; Scanducci de Freitas, P.; Scherf, U. *Adv. Mater.* **2002**, *14*, 374−378.
(59) Sinha, S.; Rothe, C.; Güntner, R.; Scherf, U.; Monkman, A. P. *Phys. Rev. Lett.* **2003**, *90*, 127402−127405.
(60) Craig, M. R.; de Kok, M. M.; Hofstraat, J. W.; Schenning, A. P. H. J.; Meijer, E. W. *J. Mater. Chem*. **2003**, *13*, 2861−2862.
(61) Nikitenko, V. R.; Lupton, J. M. *J. Appl. Phys.* **2003**, *93*, 5973−5977.
(62) Sims, M.; Bradley, D. D. C.; Ariu, M.; Koeberg, M.; Asimakis, A.; Grell, M.; Lidzey, D. G. *Adv. Funct. Mater*. **2004**, *14*, 765−781.
(63) Zhao, W.; Cao, T.; White, J. M. *Adv. Funct. Mater*. **2004**, *14*, 783−790.
(64) Yang, X. H.; Jaiser, F.; Neher, D.; Lawson, P. V.; Bredas, J.-L.; Zojer, E.; Güntner, R.; de Freitas, P. S.; Forster, M.; Scherf, U. *Adv. Funct. Mater*. **2004**, *14*, 1097−1104.